Proceedings of ASME Turbo Expo 2020
Turbomachinery Technical Conference and Exposition
GT2020
June 22-26, 2020, London, England

GT2020-15959

NUMERICAL INVESTIGATION OF THE EFFECT OF FLUTTER INSTABILITY OF THE BLADE ON THE UNSTEADY FLOW IN A MODERN LOW-PRESSURE TURBINE

Shine Win Naung[1], Mohammad Rahmati[1], Hamed Farokhi[1]

[1]Department of Mechanical and Construction Engineering, Faculty of Engineering and Environment, Northumbria University, Newcastle upon Tyne, United Kingdom, NE1 8ST

ABSTRACT

Modern aeronautical Low-Pressure Turbines (LPTs) are prone to aeroelastic instability problems such as flutter. The aerodynamic performance of a modern LPT is often influenced by the interaction between the transient flow and the dynamic behaviour of the blade. Therefore, the investigation and understanding of the physics behind the interaction between the unsteady flow and the flutter phenomenon of the blade in an LPT, which is normally left out by existing studies, is an important aspect of the research to improve the aerodynamic performance of the turbine as well as to ensure the blade mechanical integrity. In this paper, a novel analysis is conducted to explore the flutter instability in a modern LPT, T106A turbine, using two inter blade phase angles (IBPAs), and their effects on the unsteady flow field are investigated. The zero degree and 180 degrees IBPAs are considered in this paper. A high-fidelity direct numerical simulation method is used for the flow simulations. Another distinctive feature of this paper is the use of the 3D model to analyse the effects associated with the 3D blade structure and the 3D vibration mode. The investigation and identification of adequate working ranges of the harmonic balance method, which has been widely used for the aeromechanical analysis of turbomachines, are also presented in this work. This paper will bridge a key gap in the knowledge of aeroelasticity modelling and analysis of modern LPTs.

Keywords: low-pressure turbines; computational fluid dynamics, fluid-structure interaction, aeroelasticity; direct numerical simulation method; harmonic balance method

NOMENCLATURE

U	Vector of conservative variables
Ω	Fluid volume
S	Surface
$\vec{F}_I$	Inviscid flux vectors
$\vec{F}_V$	Viscid flux vectors
S_T	Source term
R	Lumped residual and source term
$\bar{U}$	Fourier coefficient of conservative variables
A_m	Fourier coefficient of conservative variables
B_m	Fourier coefficient of conservative variables
m	Number of harmonics
ω	Vibration frequency
Δt	Time-step size
h	Mesh spacing
u	Fluid velocity
C_{FL}	CFL number
C_p	Time-averaged pressure coefficient
p_w	Wall static pressure
p_{ref}	Reference pressure
$p_{t\text{-}in}$	Inlet total pressure
p_t	Total pressure
ω_u	Wake deficit
τ_w	Wall shear stress
C	Chord length
C_{ax}	Axial chord length
$IBPA$	Inter blade phase angle

W Aerodynamic work per vibration cycle
p Fluid pressure
$\vec{v}$ Velocity of the blade due to imposed displacement
$\hat{n}$ Surface normal unit vector
A Surface area
t_o Initial time
T_{Period} Period of one vibration cycle

1. INTRODUCTION

Low-Pressure Turbines (LPTs), typically found in modern civil aero engines and gas turbine engines, weight approximately 20-30 percent of the total engine weight [1]. The high blade loadings and the flow separation due to a low Reynolds number are typical features of a modern LPT, and the interaction between the transient flow and the blade structure in an LPT can have a significant influence on the aerodynamic performance of the turbine. A number of studies have been conducted to maximise the performance of LPTs and a high level of efficiency, 90-93 percent, has been achieved as a result [2].

Reducing the weight of LPTs in aero engines and gas turbines and their associated manufacturing costs have been the main focus of the research industry after a high level of efficiency has been obtained [3]. A 'high-lift' blade design, which increases the required aerodynamic loads on the blade but using fewer blades, is one of the outcomes [4]. However, this design not only decreases the highly correlated LPT flutter parameter known as reduced frequency but also introduces the higher per-stage loading [5-7], potentially leading to aeroelastic instabilities such as flutter as a result of a high aspect ratio of the blade [8]. Many structural failures of the blade of LPTs are directly associated with aeroelastic instability problems [9]. Therefore, the assessment and understanding of the physics of the flutter instability of LPTs are required to ensure the blade mechanical integrity.

An accurate prediction of flutter instability in turbomachines, especially in LPTs, remains one of the greatest unsolved challenges in the industry. Several studies have been conducted over the last decades to seek efficient and effective numerical methods. One of them is the time-linearized harmonic frequency-domain method which has been developed and widely used for turbomachinery aeromechanical applications [10-11]. However, these methods were superseded by the harmonic balance method of Hall et al. [12], the phase solution method of He [13], and Rahmati et al. [14-15] which provide a particularly elegant way of modelling harmonic disturbances. Rahmati et al. [16] developed a nonlinear frequency domain solution method for the turbomachinery aeromechanical analysis and design of multiple blade row configurations. It is shown that a fully coupled multi-row analysis should yield more accurate flutter predictions than the simplified isolated blade row case [17]. Shine et al. [18-19] also applied the non-linear harmonic method to the aerodynamic and aeromechanical analysis of wind turbine rotors.

The existing high-fidelity aeroelastic solvers are based on the Unsteady Reynolds Averaged Navier–Stokes (URANS) models. However, the URANS models are unable to accurately predict the behaviour of the unsteady flow, especially in the flow separation zones, due to the inadequacy of turbulence models [20-22]. Therefore, the required confidence and accuracy cannot be obtained with the URANS models when the highly unsteady flow and the flow separation, which are seen in LPTs, are involved. The existing aeroelastic models and solvers used in the industry mainly focus on aeroelasticity parameters such as the value of aerodynamic damping and disregard the complex physics occurring during the fluid-structure interaction process which gives rise to a black-box effect. As a result, the understanding of the interaction between the various sources of unsteadiness and the blade structure is still limited, and it requires further investigations. Therefore, high-fidelity numerical methods and models are required to further investigate the physics behind the interaction between the unsteady flow field and the flutter behaviour of the blade.

This paper aims to assess the flutter instability in a modern LPT using a high-fidelity Direct Numerical Simulation (DNS) method in which the various sources of unsteadiness associated with the fluid-structure interaction are included. To the best of the authors' knowledge, most research to date have focused only on the transient flow and flow separation at the blade mid-span of modern aeronautical LPTs. The 3D model is used in this paper and the effects associated with the 3D blade structure are investigated. Two inter blade phase angles (IBPAs), zero degree and 180 degrees, are used in the present simulations and their effects on the unsteady flow field are analysed and discussed in this paper. These phase angles are particularly chosen to investigate the completely in-phase and out-of-phase scenarios between two adjacent blades. This work will provide fundamental understandings of the mechanism behind the interaction between the flow field unsteadiness and the blade structure in a modern LPT. Adequate working ranges of the harmonic balance method, which has been widely used for the aeroelasticity analysis of turbomachines, are also investigated and identified in this paper. This work will bridge a key gap in the knowledge of aeroelasticity modelling and prediction of turbomachines.

2. T106A LINEAR TURBINE CASCADE

2.1 Description of the T106A Turbine

The highly loaded T106A linear turbine cascade has been selected for the present study. This turbine has been studied both experimentally [23] and numerically [24-31]. The experimentally studied test rig consists of seven aft-loaded blades. The blade aspect ratio and pitch-to-chord ratio are 1.76 and 0.799, respectively. The experimental measurements of this turbine were performed at a relatively low Reynolds number of 51,800 with an inflow angle of 37.7 degrees. The required Reynolds number is obtained based on the inflow speed and the axial chord length in the present simulations. However, it should be noted that the inflow angle

for the numerical simulations is shifted to 45.5 degrees due to some uncertainties in the experiment as explained in [30-31]. The time-averaged pressure coefficient distribution and the wake loss profile in a cross-section downstream of the blade trailing edge were measured during the experiment, and they will be compared to the numerical results for validation purposes. In addition, the wall shear stress on the blade surfaces is also computed and compared to the previous DNS simulation. Titanium Alloy is considered to be the material of the blade in this study and it has a density of 4620 kg/m^3, Young's modulus of 9.6E+10 Pa and Poisson's ratio of 0.36.

2.2 Computational Domain and Grid

The complete 3D model including the hub and the shroud is considered for the present simulations to analyse the effect of the 3D blade vibration on the flow. The span of the blade is 2.5C_{ax}, where C_{ax} is the axial chord length. The pitch length is 0.9306C_{ax}. The computational grids are generated using a structured grid generator based on structured multi-block techniques. The O4H topology is used to create the mesh which includes five blocks – the skin block which is an O-mesh surrounding the blade, the inlet block which is an H-mesh located upstream of the leading edge, the outlet block which is an H-mesh located downstream of the trailing edge, the upper block which is an H-mesh located above the blade section, and the lower block which is an H-mesh located under the blade section. The mesh in the skin block, the upper block, the lower block and the outlet block are significantly refined to resolve the necessary flow structures. As a steady inflow is only considered in this study, a coarser mesh has been generated in the inlet block to reduce the total number of cells and the computation time. The grid point distributions in the stream-wise, pitch-wise and span-wise directions in the skin block, the upper block, the lower block and the outlet block are 385x33x97, 393x29x97, 393x29x97 and 225x49x97, respectively, whereas that of the inlet block is 25x49x97. The first layer thickness which is the width of the first cell close to the wall is 1e-5 meters leading to the non-dimensional wall distance, y^+ value, less than 1. The mesh has the total grid points of 4.5 million in a single passage. Two IBPAs, zero degree and 180 degrees, are considered in the present work. A single passage is used for the zero degree IBPA case and an additional passage is added on the top of the referenced passage in the case of 180 degrees IBPA. Figure 1 shows the computational grid at the blade mid-span section of a single passage.

2.3 Computational Methodology

The analysis of unsteady flow using the stationary blade is initially performed to validate the CFD model. After validation, the blade is imposed a vibration with a frequency and amplitude to initiate the flutter instability in T106A turbine and to analyse the interaction between the transient flow and the blade structure vibration. The modal analysis is conducted before the flow simulation to compute the natural frequencies and the structural mode shapes of the blade. The first vibration mode is used for the blade vibration in which the first natural frequency is defined to be the vibration frequency. Both the time domain method and the harmonic balance method are used for the unsteady simulations using the vibrating blade. By using the same numeric for both methods, the capability of the harmonic balance method on analysing the flutter instability in modern LTPs involving highly unsteady flow and wake can be determined. The flow simulations are conducted using the DNS method.

For the flow simulation, the flow is governed by the unsteady Navier-Stokes equations and the general Navier-Stokes equations written in a Cartesian frame can be expressed as:

$$\frac{\partial}{\partial t}\int_\Omega U d\Omega + \int_S \vec{F_I} \,.\, d\vec{S} + \int_S \vec{F_V} \,.\, d\vec{S} = \int_\Omega S_T d\Omega \qquad (1)$$

where Ω is the volume, S is the surface, U is the vector of the conservative variables, S_T is the source term, and $\vec{F_I}$and $\vec{F_V}$are the inviscid and viscous flux vectors, respectively. The above equation can be simply written in a semi-discrete form as:

$$\frac{\partial}{\partial t}(U) = R(U) \qquad (2)$$

where R is the lumped residual and the source term. With the DNS method, the Navier-Stokes equations are directly solved without any turbulence model. The commercially available three-dimensional pressure-based finite volume solver, ANSYS CFX, is used in the present study. The pseudo-time marching approach is used for the steady-state solution. For the unsteady solution, the advection terms are discretized using a bounded high-resolution advection scheme and the temporal derivatives are discretized using a 2nd order backwards Euler approximation for the time domain method.

In this study, the harmonic balance method is also implemented with a pressure-based solution approach. With this method, the transient flow variables, U, are represented by a Fourier series for a prescribed fundamental frequency, ω, and the specified number of harmonics, m, as expressed in Eq. (3).

$$U = \bar{U} + \sum_{m=1}^{M}[A_m \sin(m\omega t) + B_m \cos(m\omega t)] \qquad (3)$$

where $\bar{U}$, A_m, and B_m are the Fourier coefficients of the conservative variables. Substituting Eq. (3) into Eq. (2) yields the following equations.

$$\omega \sum_{m=1}^{M}[mA_m \cos(\omega t) - mB_m \sin(\omega t)] = R \qquad (4)$$

The unsteady period is equally divided into $N = (2m+1)$ time levels and the system of nonlinear equations coupling all N time levels are solved iteratively. In this method, the time derivatives are evaluated using the spectral approximation.

To resolve the unsteady flow accurately, the time step size, Δt, must be small enough such that a fluid particle moves only a fraction of the mesh spacing h with fluid velocity u in each step, and it is given by:

$$\Delta t = C_{FL} \frac{h}{u} \quad (5)$$

where C_{FL} is the CFL number and it is kept to a value less than one.

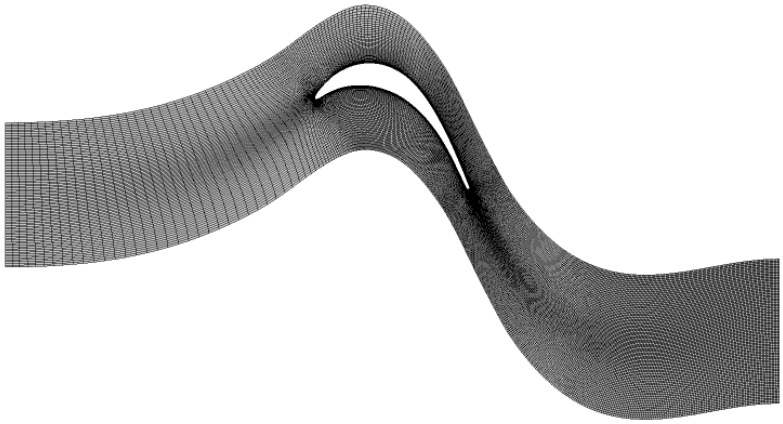

FIGURE 1: COMPUTATIONAL GRID AT THE BLADE MID-SPAN OF THE T106A TURBINE

2.4 Boundary Conditions

The inlet velocities in Cartesian components, as explained in [27], are applied at the inlet to achieve the required inflow angle of 45.5 degrees and the desired Reynolds number of 51,800. The pressure outlet boundary condition is defined at the outlet. The solid wall boundary conditions are applied on the blade surfaces. As the hub and the shroud are also present in this study, they are treated as wall boundaries, and the periodic boundary conditions are applied in the pitch-wise direction. As two passages are involved in the 180 degrees IBPA case, the general connection interface model, available in ANSYS CFX, is used to connect the two passages. This interface is used to collect and exchange the flow information between the two passages and the flow data are then transferred to the periodic boundaries.

3. RESULTS

3.1 Analysis of Unsteady Flow using the Stationary Blade

Before analysing the effect of the flutter instability on the unsteady flow, the unsteady simulation using the stationary blade is first conducted to validate the CFD model. The numerical results are compared to the experiment as well as the reference DNS simulations for validation. The results discussed are extracted at the blade mid-span section. The time-averaged static pressure coefficient, C_p, can be defined as $(p_w - p_{ref})/(p_{t\text{-}in}\text{-}p_{ref})$, where p_w is the blade wall static pressure, p_{ref} is the reference outlet pressure, and $p_{t\text{-}in}$ is the inlet total pressure. The time-averaged C_p distribution computed from the present simulation is compared to the experiment as well as the previous DNS simulation performed by Wissink et al. [27], and they are presented in Fig. 2. As seen, the results obtained are in very good agreement with the experiment as well as the reference DNS simulation.

The wake loss profile, also called as wake deficit, ω_u, can be defined as $(p_{t\text{-}in}\text{-}p_t)/(p_{t\text{-}in}\text{-}p_{ref})$, where p_t is the total pressure, and it is computed at 40% chord downstream of the blade trailing edge. Similar to C_p, the time-averaged wake loss profile from the present simulation is compared to the experiment as well as the DNS simulation conducted by Michelassi et al. [30], and they are shown in Fig. 3. It is seen that the studied 3D model captures the wake loss reasonably well, but the peak location is slightly different from the experiment. The reason for this is not very clear, as discussed in [25,30], but it can be related to the fact that a small inflow turbulence intensity was noted during the experiment. Nevertheless, the mesh used in this study is considered fine enough for further investigations involving blade vibration.

In addition to the pressure coefficient distribution and the wake loss profile, the shear stresses on the blade surfaces are also computed in this study, and the results are compared to the previous DNS simulation performed by Michelassi et al. [30]. Figure 4 demonstrates the comparison of the wall shear stresses between the present simulation and that of Michelassi et al. [30]. It should be noted that inflow turbulence was introduced in the simulation of Michelassi et al. As shown, they are in very good agreement although a little difference is seen near the trailing edge. However, this is due to the difference in inflow turbulence between the two simulations. A clean inflow is used in the present simulation. Therefore, it is concluded that the CFD model used in the present study is valid for further investigations after having obtained the results which agree well with the experiment as well as the reference DNS simulations.

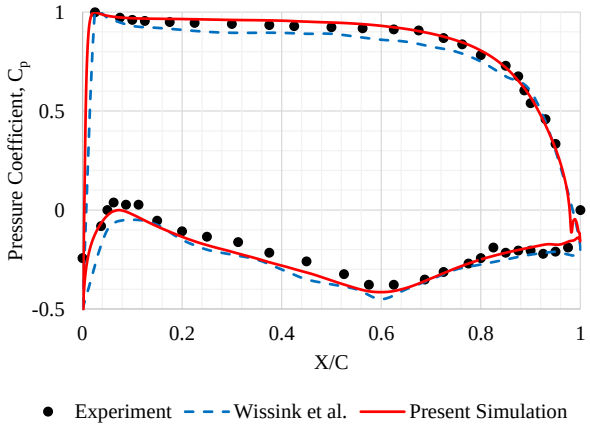

FIGURE 2: TIME-AVERAGED PRESSURE COEFFICIENT DISTRIBUTIONS

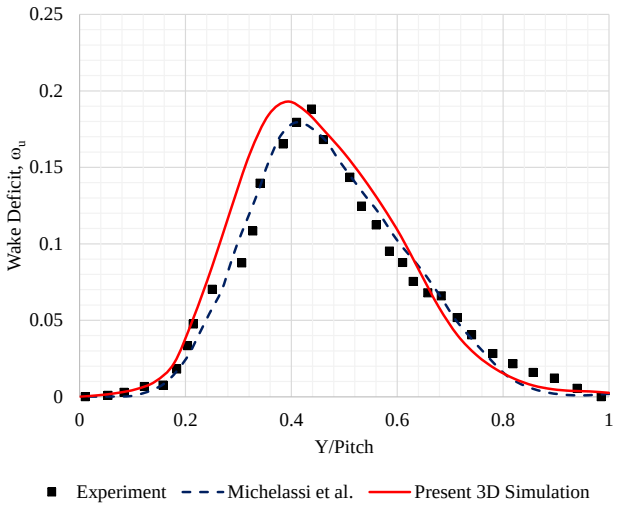

FIGURE 3: WAKE LOSS PROFILES

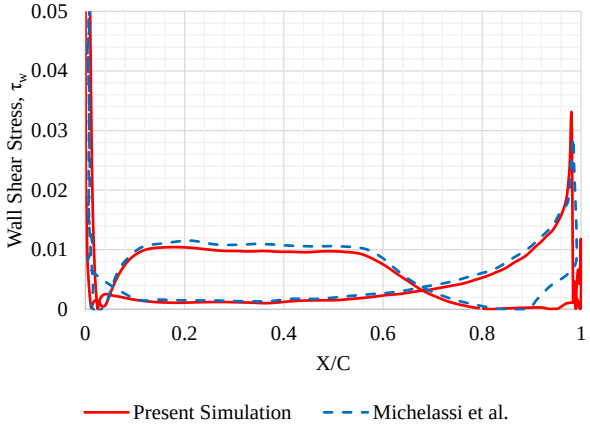

FIGURE 4: WALL SHEAR STRESS

As the emphasis of this paper is to analyse the unsteady flow mechanism due to interaction with the blade, it is important to determine whether the employed model can capture the necessary flow structures. Figure 5 illustrates the instantaneous vorticity fields at the blade mid-span at four equally spaced instants, where t is the local time step and T is the total run time. Although a single passage domain is simulated for this analysis, the additional two passages are added and shown for better visualisation of the flow structures. The flow separates in the aft region on the suction surface of the blade before shedding from the trailing edge, whereas the flow remains laminar and attached on the pressure surface. Laminar vortex shedding from the trailing edge, of which the flow structures are similar to that of Karman vortex, is dominant within the initial periods. The separation of shear layers and the evolution of coherent structures are observed as time goes on. The rolling up and breaking down of separated shear layers due to Kelvin-Helmholtz instability leads to a transition to the turbulence near the trailing edge. After a certain period, the flow structure is stretched near the trailing edge and the organized mushroom-like vortex structures are developed in the downstream region resulting in the highly unsteady and fully turbulent downstream wakes. Therefore, it can be noted that the numerical model used in this paper captures the unsteady flow structures and can be used for further analysis.

3.2 Analysis of the Flutter Instability of the Blade on the Unsteady Flow

The main objective of this paper is to assess the flutter instability in a modern LPT and to analyse their effects on the unsteady flow field. The first vibration mode, of which the first natural frequency is 250 Hz, is used and prescribed in the flow simulation. The first natural frequency is set to be the vibration frequency in this study. The maximum vibration amplitude is defined to be 3%C_{ax} at the tip of the blade in this study so that the amplitude at the blade mid-span section is approximately 1%C_{ax}. This will also allow visualising the flow structures relating to relatively large amplitude. Two IBPAs, zero degree and 180 degrees, are used in this paper to investigate the effects associated with the different IBPAs. The mode shape of the T106A turbine blade is demonstrated in Fig. 6.

The time-averaged pressure coefficient distributions on the surfaces of the reference blade, the lower blade, obtained from the two cases using different IBPAs are compared to the stationary blade case to investigate the effects of vibration with different IBPAs, and they are presented in Fig. 7 and 8. As seen, in the case of 180 degrees IBPA, there is a significant impact on the reference blade due to the change in pitch length between the blades within a vibration cycle. The impact is much greater in the blade outer region close to the shroud, especially near the trailing edge where the vibration amplitude is maximum, as the flow is most disturbed by those from the other blade sections as well as the neighbouring blades. The similar nature is also observed in the zero degrees IBPA case but the flow disturbance by the neighbouring blades is less compared to the 180 degrees case. In both zero and 180 degrees cases, slight differences are seen in the blade inner region where the vibration amplitudes are small.

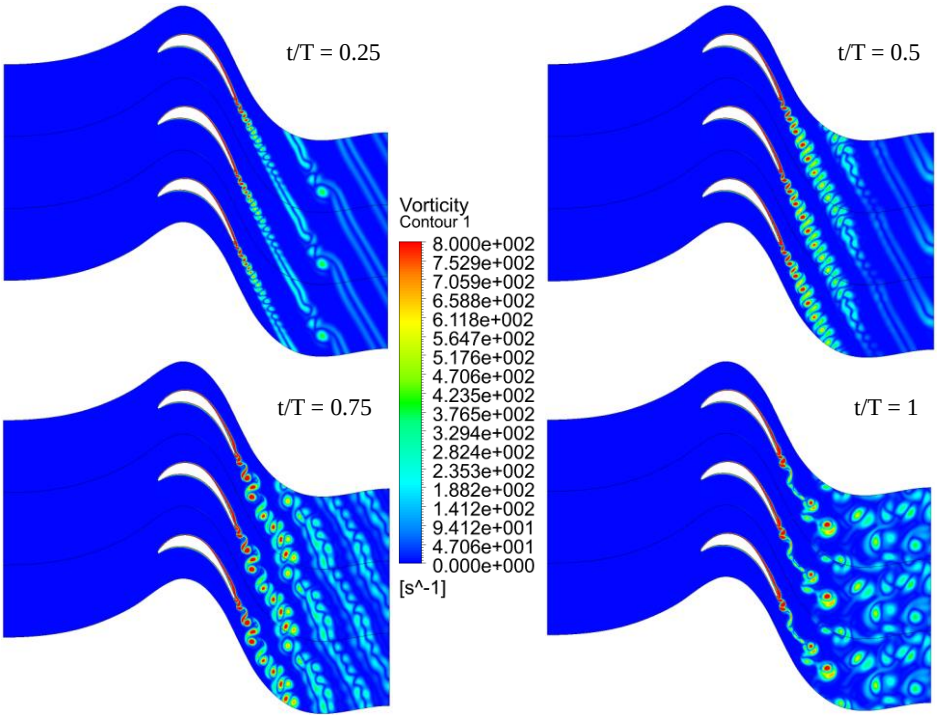

FIGURE 5: INSTANTANEOUS VORTICITY FIELDS AT THE BLADE MID-SPAN

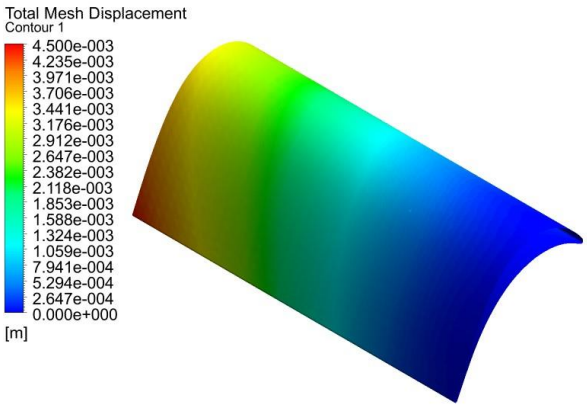

FIGURE 6: FIRST VIBRATION MODE OF THE T106A TURBINE BLADE

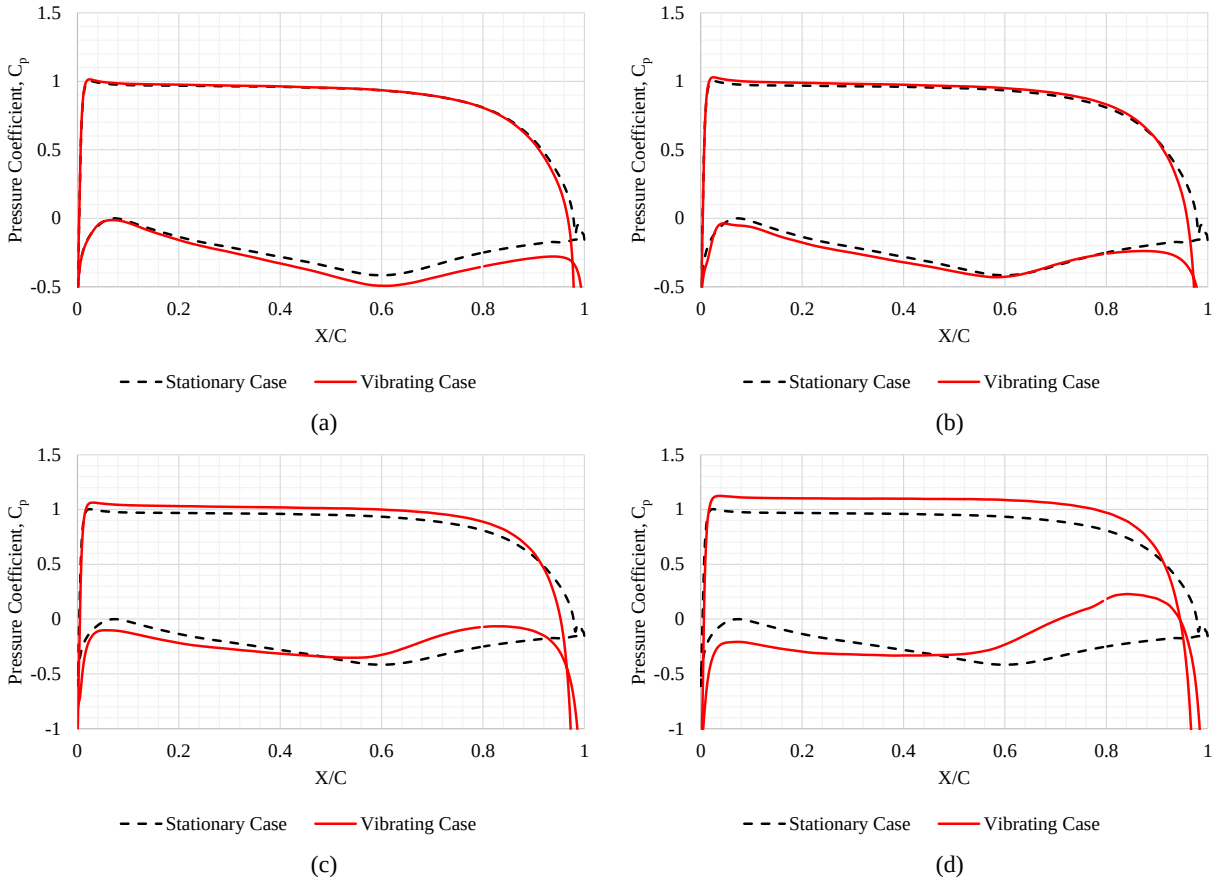

FIGURE 7: TIME-AVERAGED PRESSURE COEFFICIENTS AT (A) 30%, (B) 50%, (C) 70%, AND (D) 90% SPAN BLADE SECTIONS FROM THE ZERO DEGREE IBPA CASE

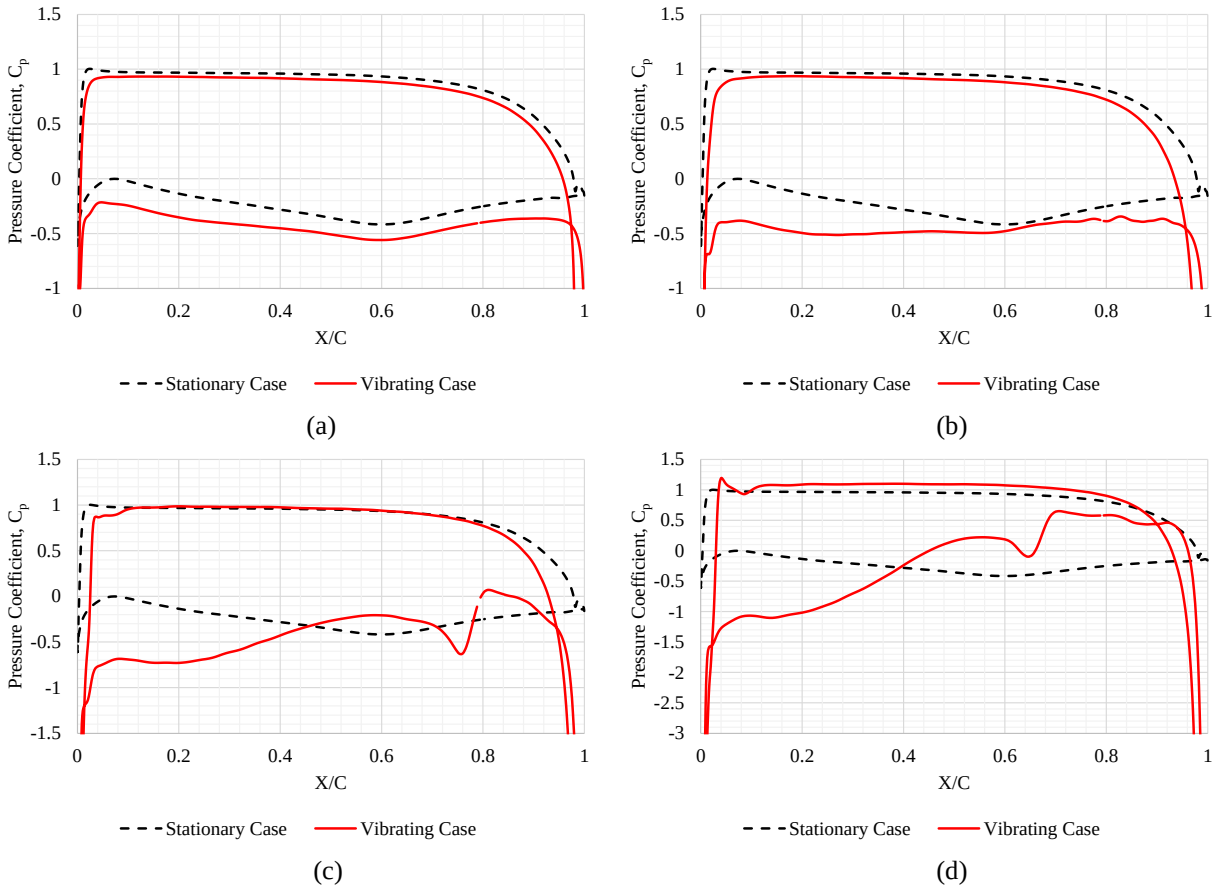

FIGURE 8: TIME-AVERAGED PRESSURE COEFFICIENTS AT (A) 30%, (B) 50%, (C) 70%, AND (D) 90% SPAN BLADE SECTIONS FROM THE 180 DEGREES IBPA CASE

Figure 9 illustrates the wake profiles, obtained from the zero degree IBPA case and the 180 degrees IBPA case, computed at 40% chord downstream from the blade trailing edge at the blade mid-span of the lower blade passage. The wake profile from the stationary blade case is also added to the comparison to see the differences between the stationary blade case and the vibrating blade case. A complete difference in wake profiles is seen between two IBPA cases and the stationary blade case which show that the blade vibration has a significant impact on the unsteady flow downstream. The magnitudes of wake profiles are much larger in the vibrating blade cases compared to the stationary blade case. The wake profile is a total opposite of the stationary blade case in the zero degree IBPA case whereas, in the case of 180 degrees IBPA, a sinusoidal-like pattern of wake profile is observed. The total pressure rise after about 80% pitch in the latter case is associated with the flow disturbances from the upper blade passage. These disturbances can be visualised in Fig. 10 which shows the total pressure distributions for the two IBPA cases.

Figure 11 and 12 demonstrate the evolution process of vorticity at the blade mid-span over the vibration periods for the two IBPA cases. The vortex structures are produced as soon as the blade starts vibrating, and the initially produced vortex structures are pushed away by the latterly produced ones in both cases. As shown in Fig. 11, in the case of zero degree IBPA, a recurring pattern of vortex formation can be seen over the vibration periods and the vortex structures produced by the upper blade start mixing up with those from the lower blade after about 10 vibration periods. The turbulent flow field and wake can be observed in the downstream region after 20 vibration periods. On the other hand, the flow behaviour is different in the case of 180 degrees IBPA (see Figure 12). The vortex structures from the upper blade seem to go down and approach those from the lower blade, which is also consistent with the wake profile and total pressure distribution as previously seen, and the turbulent flow field is formed soon after they departed from the blade trailing edge. At about the 15 vibration-period, the rolling up of vortex structures and a flow separation can be noticed on the suction surface of the blade due to the change in pitch length between the blades within the vibration cycle. This effect is much greater after about 20 vibration periods.

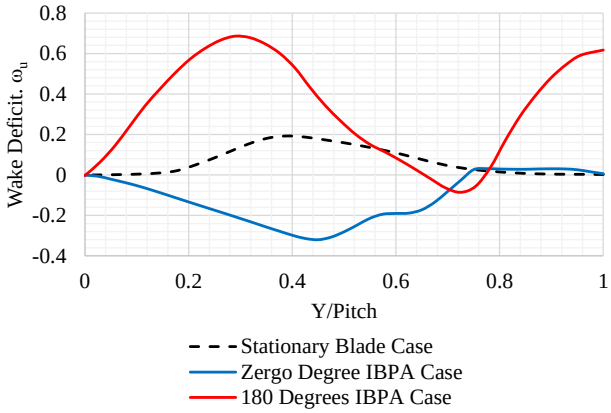

FIGURE 9: WAKE PROFILES

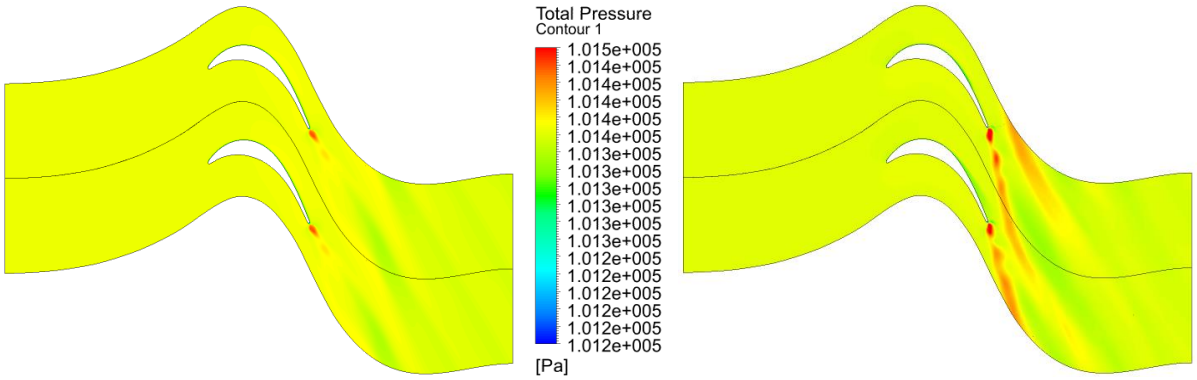

(a) (b)

FIGURE 10: TOTAL PRESSURE CONTOURS FROM (A) ZERO DEGREE AND (B) 180 DEGREES IBPA CASES AT THE BLADE MID-SPAN

Figure 13 and 14 illustrate the vorticity fields at different blade sections, obtained after 20 vibration periods, from the two studied cases to visualise the effect of different vibration phase angles on the flow at different blade sections. The flow fields are very similar at the 30% span blade section where the amplitude of vibration is very small and hence the effect of the IBPA is not significant. However, a noticeable difference between the two cases is observed at the blade mid-span. The vortex structures from the upper blade come down and mix up with those from the lower blade soon after they departed from the blade trailing edge in the 180 degrees IBPA case whereas a similar pattern of vortex structures with the flow mixing up in the far downstream region is seen in the zero degree IBPA case. At the blade outer sections, the flow mixing up occurs as early as they shed from the trailing edge in both cases. However, the flow unsteadiness and turbulence are higher in the case of 180 degrees IBPA. Therefore, conclusions can be drawn from these observations that the blade vibration has a significant impact on the unsteady flow field and the flow behaviour strongly depends on the IBPA.

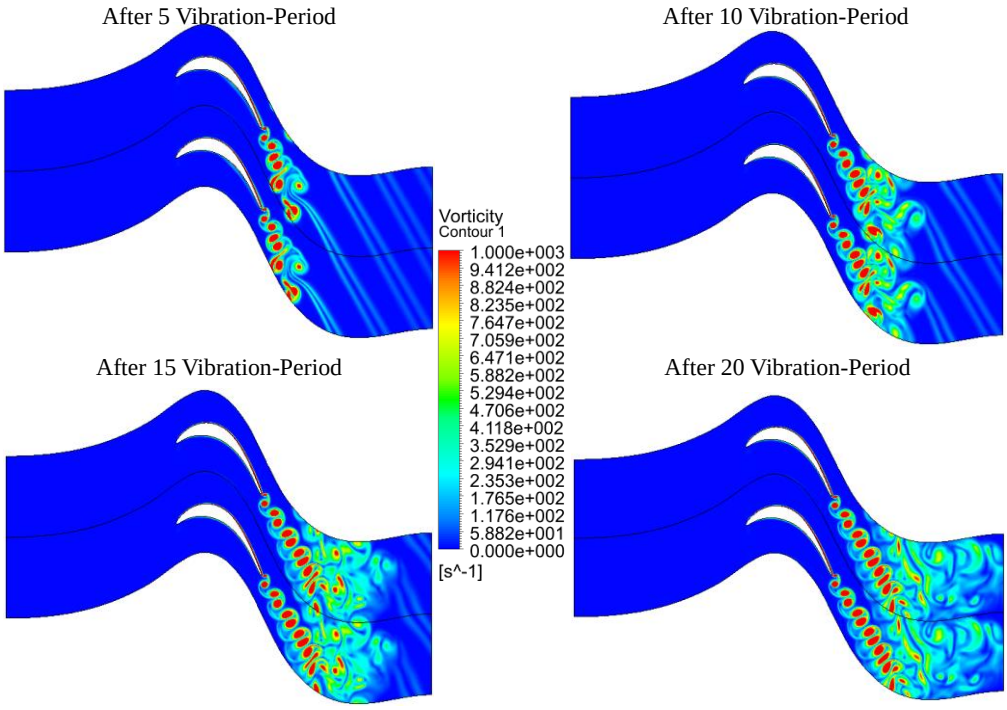

FIGURE 11: EVOLUTION PROCESS OF VORTICITY OVER THE VIBRATION PERIODS AT THE BLADE MID-SPAN IN THE ZERO DEGREE IBPA CASE

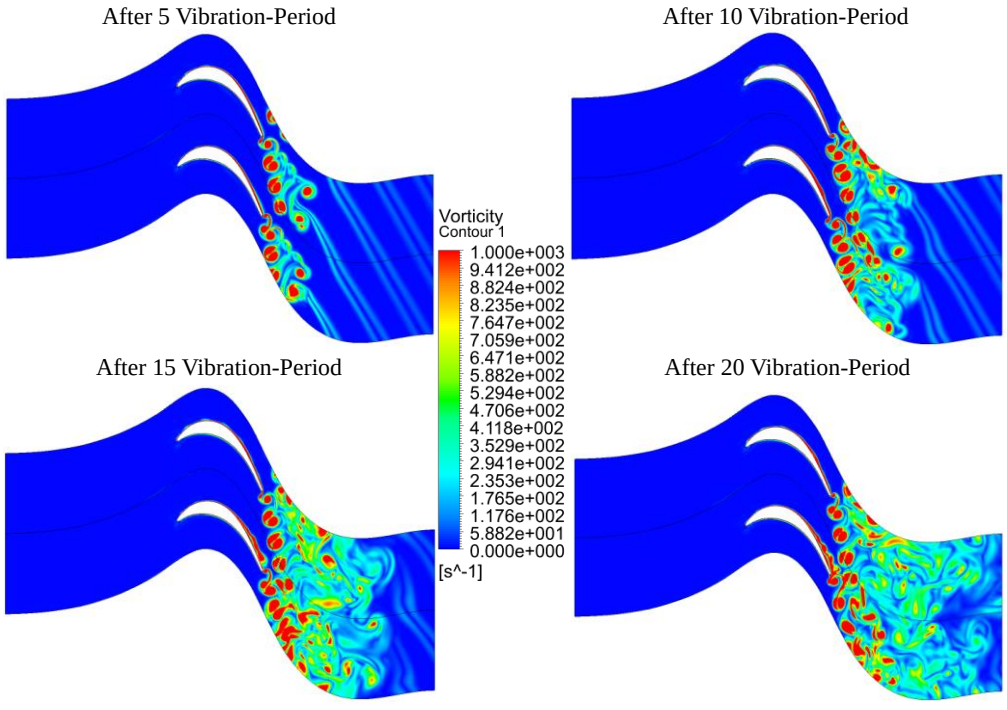

FIGURE 12: EVOLUTION PROCESS OF VORTICITY OVER THE VIBRATION PERIODS AT THE BLADE MID-SPAN IN THE 180 DEGREES IBPA CASE

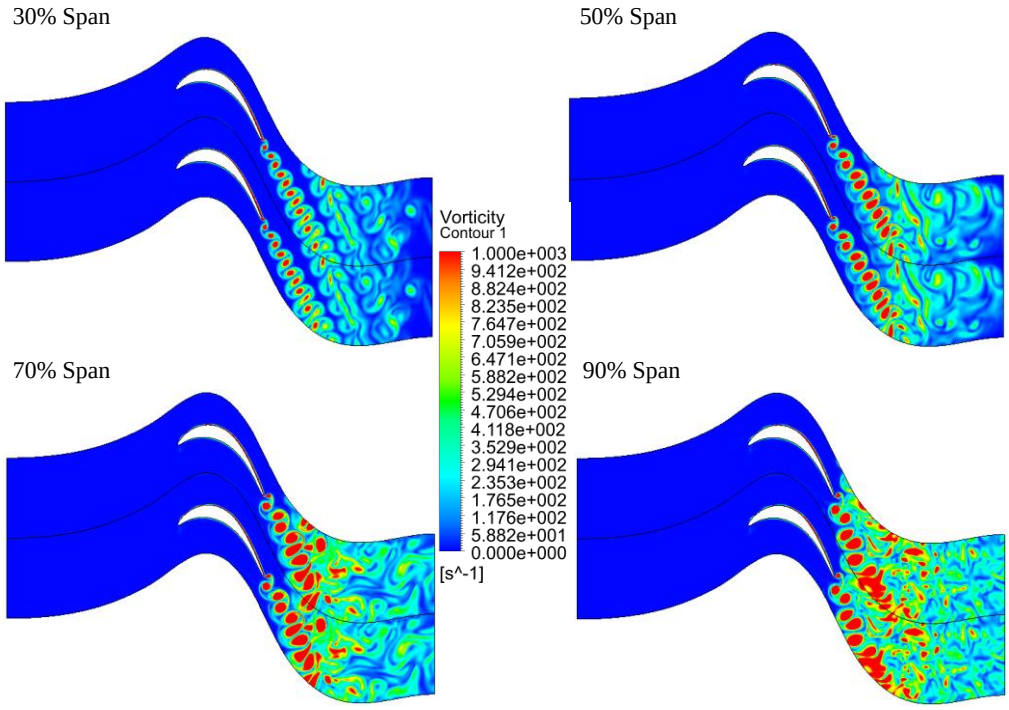

FIGURE 13: VORTICITY FIELDS AT DIFFERENT BLADE SECTIONS IN THE ZERO DEGREE IBPA CASE

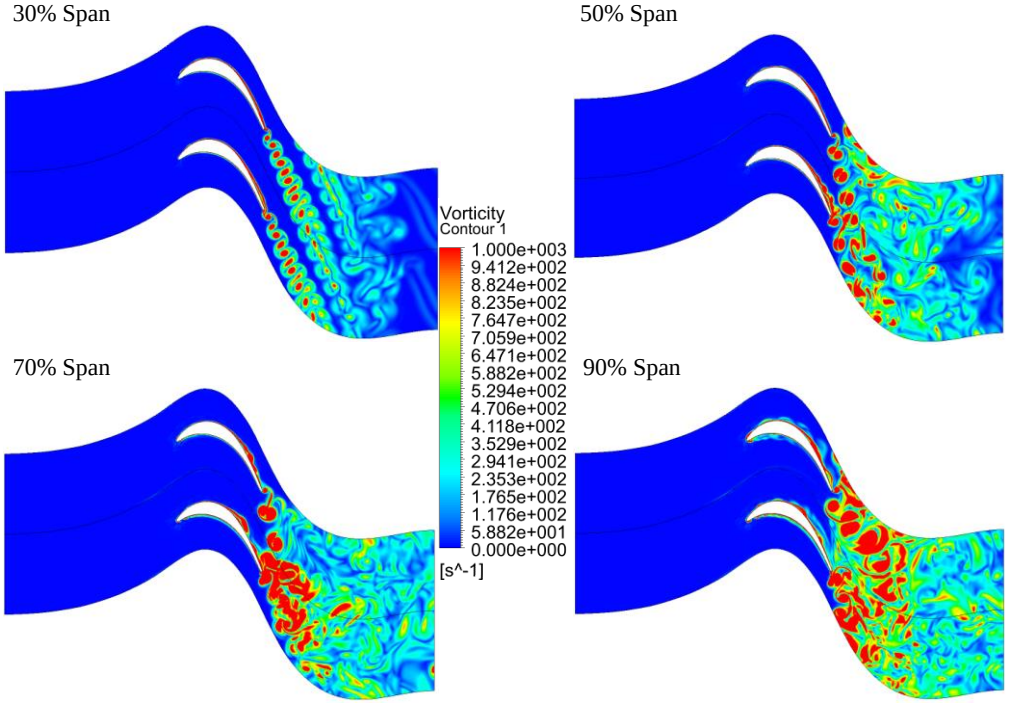

FIGURE 14: VORTICITY FIELDS AT DIFFERENT BLADE SECTIONS IN THE 180 DEGREES IBPA CASE

In addition to the time domain method, the harmonic balance method with different harmonics is also used in this analysis to determine its capability on analysing the aeroelastic instabilities and the unsteady flow in an LPT at low Reynolds number. The vorticity fields predicted by different methods for both cases are presented in Fig. 15 and 16. As shown, the vorticity captured by the harmonic balance method using 1 harmonic and 3 harmonics are not comparable to that of the time domain method. This means that 3 harmonics are not enough to resolve the flow structures. Using 5 harmonics seems to have captured the similar vortex structures as the time domain method. Therefore, it can be said that at least 5 harmonics are required to resolve the necessary flow structures in these cases. Fig. 17-20 show the unsteady pressure amplitude coefficient and phase angle, extracted at 30% span and 90% span, obtained from the time domain method and the harmonic balance method using 5 harmonics. As seen, the results obtained from both methods agree well with each other. Computational resources required by using 5 harmonics and 3 harmonics are three times and two times more than that of using 1 harmonic, respectively. Although the flow resolution will be better with higher

numbers of harmonics, using more harmonics will result in increasing the requirement of computational resources by a significant factor, which is not preferable and sometimes can exceed the capability of powerful computers.

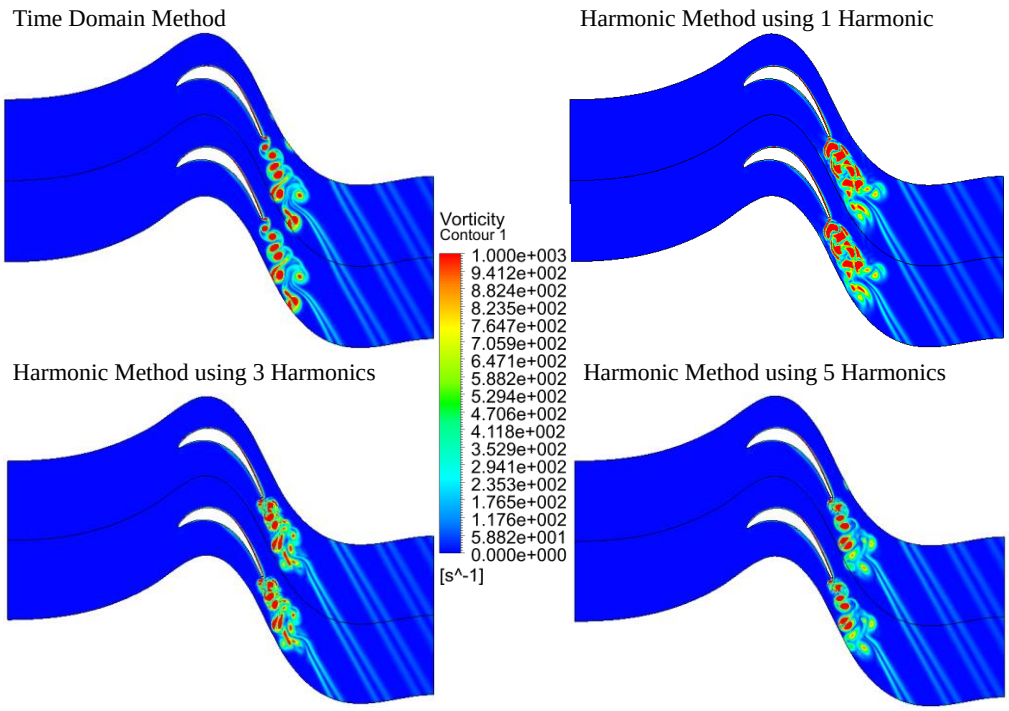

FIGURE 15: VORTICITY FIELDS PREDICTED BY DIFFERENT METHODS IN THE ZERO DEGREE IBPA CASE

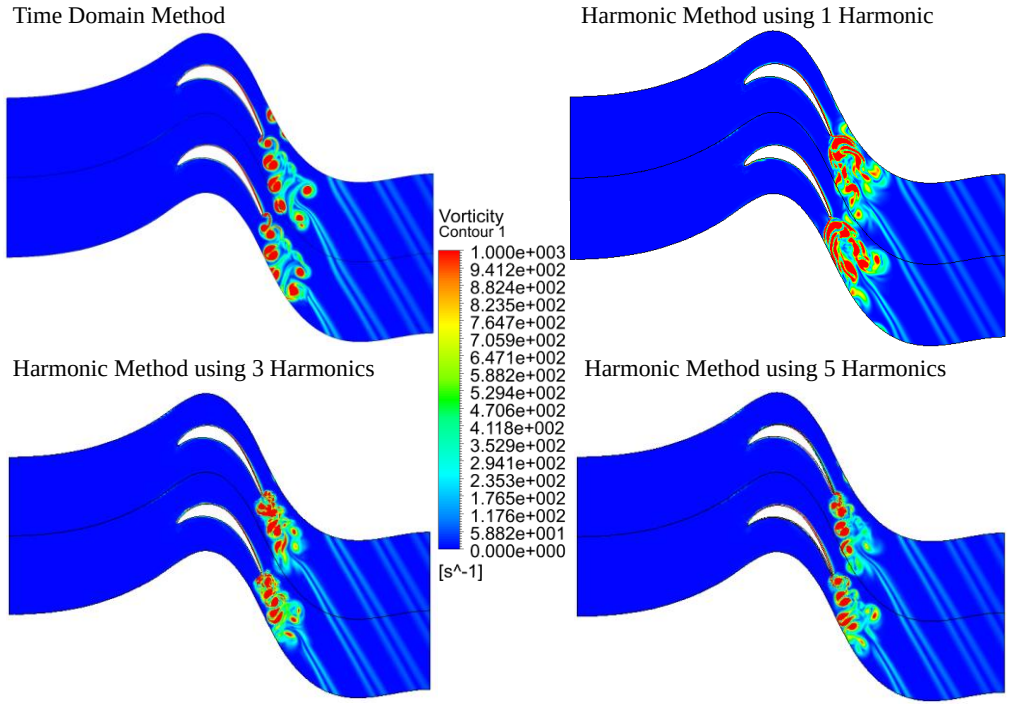

FIGURE 16: VORTICITY FIELDS PREDICTED BY DIFFERENT METHODS IN THE 180 DEGREES IBPA CASE

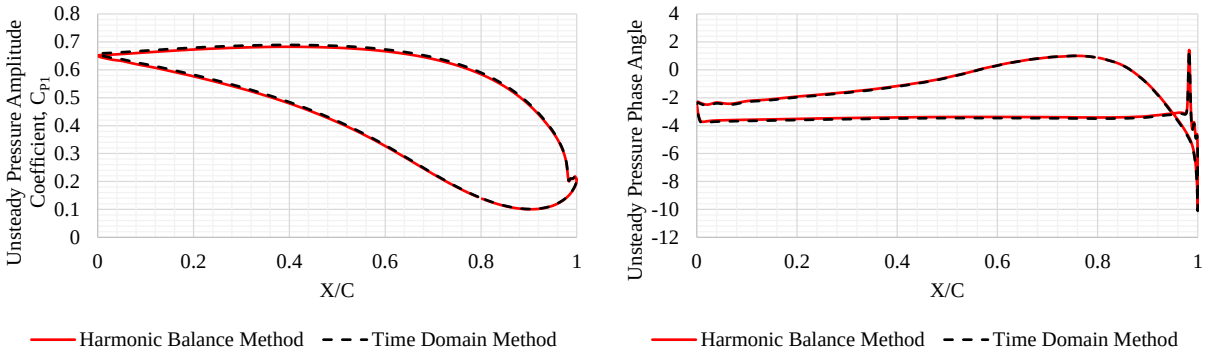

(a) (b)

FIGURE 17: (A) UNSTEADY PRESSURE AMPLITUDE COEFFICIENT AND (B) PHASE ANGLE AT 30% SPAN AT IBPA=0

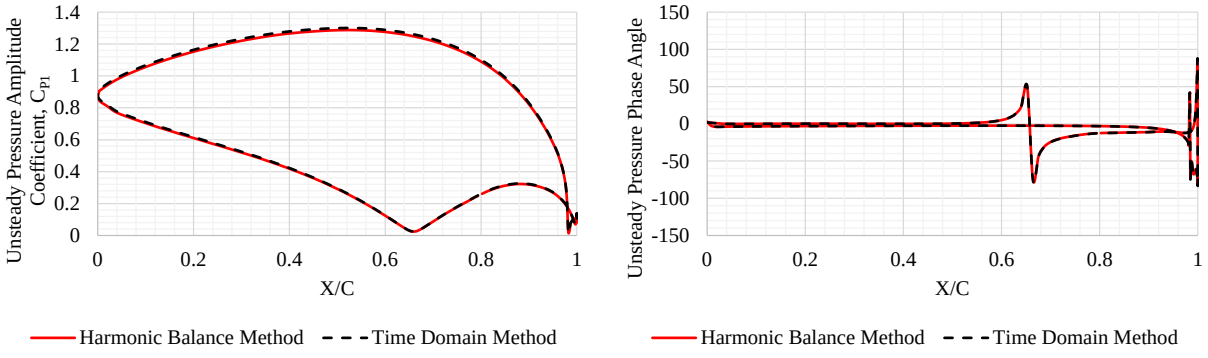

(a) (b)

FIGURE 18: (A) UNSTEADY PRESSURE AMPLITUDE COEFFICIENT AND (B) PHASE ANGLE AT 90% SPAN AT IBPA=0

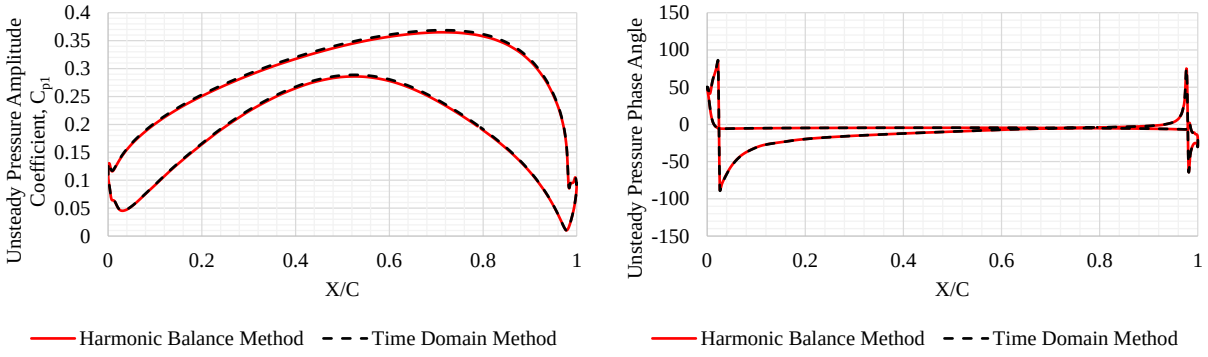

(a) (b)

FIGURE 19: (A) UNSTEADY PRESSURE AMPLITUDE COEFFICIENT AND (B) PHASE ANGLE AT 30% SPAN AT IBPA=180

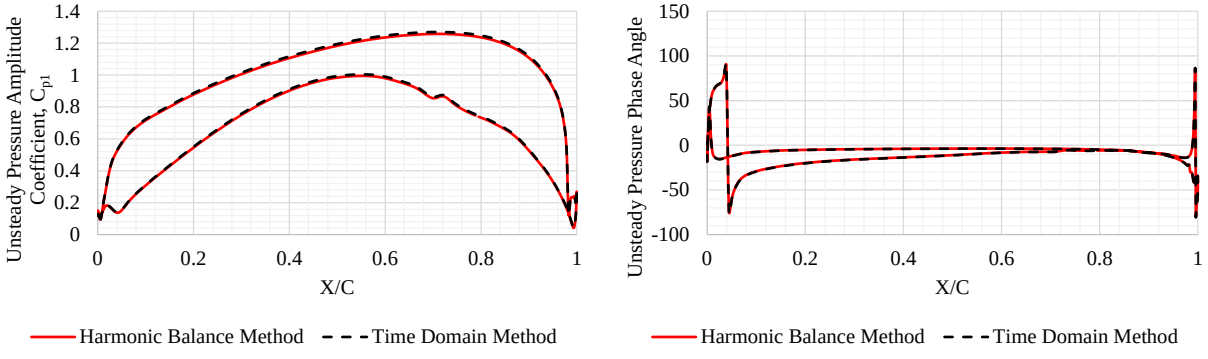

(a) (b)

FIGURE 20: (A) UNSTEADY PRESSURE AMPLITUDE COEFFICIENT AND (B) PHASE ANGLE AT 90% SPAN AT IBPA=180

TABLE 1: AERODYNAMIC DAMPING IN LOG-DEC FORM

Case	**Time Domain Method**	**Harmonic Balance Method**
Zero Degree IBPA	0.027	0.025
180 Degrees IBPA	0.053	0.050

TABLE 2: COMPUTATIONAL COST

Method	No. of Processors	CPU Cost
Time Domain Method (1 Passage)	224	43 Hours
Time Domain Method (2 Passages)	224	60 Hours
Harmonic Balance Method using 1 Harmonic (1 Passage)	32	2.5 Hours
Harmonic Balance Method using 3 Harmonics (1 Passage)	32	4.5 Hours
Harmonic Balance Method using 5 Harmonics (1 Passage)	32	6 Hours
Harmonic Balance Method using 1 Harmonic (2 Passages)	32	4 Hours
Harmonic Balance Method using 3 Harmonics (2 Passages)	32	9 Hours
Harmonic Balance Method using 5 Harmonics (2 Passages)	32	14 Hours

One of the most important parameters in the aeromechanical analysis is the aerodynamic damping value which is calculated based on the aerodynamic work done by the blade on the fluid over the vibration period. The aerodynamic work per vibration cycle can be expressed as:

$$W = \int_{t_0}^{t_0+T_{Period}} \int_A p\vec{v}.\hat{n}dAdt \qquad (6)$$

where t_0 is the initial time, T_{Period} is the period of one vibration cycle, p is the fluid pressure, $\vec{v}$ is the velocity of the blade due to the imposed displacement, A is the blade surface area, and $\hat{n}$ is the surface normal unit vector. If the aerodynamic damping value is positive, the vibration is damped for the frequency being studied. The aerodynamic damping values in the form of Log-Dec for two IBPA cases, computed from the time domain method and the harmonic balance method, are presented in Table 1. As shown, the aerodynamic damping values are positive in both cases, but it is slightly larger in the 180 degrees IBPA case. The results obtained from the two methods are in good agreement. Fig. 21 illustrates the aerodynamic damping values for various IBPAs. As the computational cost required by the time domain method to calculate the aerodynamic damping for various IBPAs is significantly high, the harmonic balance method is employed to produce Fig. 21. It is observed that the aerodynamic damping values are positive at all IBPAs considered in this study indicating that the blade vibration is stable. The aerodynamic damping is larger at higher angles.

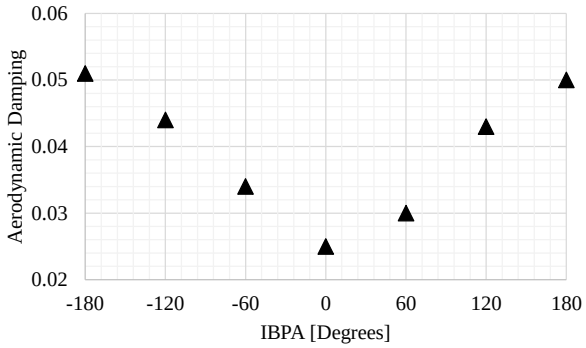

FIGURE 21: AERODYNAMIC DAMPING FOR VARIOUS IBPAS

3.3 Computational Cost

The simulations discussed in this paper are all performed on an HPC cluster. 224 processors are used for the time domain method whereas 32 processors can only be used with the harmonic balance method due to extremely large memory requirement. This can be noted as the limitation of the harmonic balance method. The computational costs with respect to the total processors used for each case are listed in Table 2. The 180 degrees IBPA case requires much more CPU time than the zero degree one for the same run time as two passages are used. The harmonic balance method solves significantly faster than the time domain method. The solution takes longer with an increasing number of harmonics. The 180 degrees IBPA case takes 14 hours on 32 processors with the harmonic balance method using 5 harmonics whereas it takes about 60 hours on 224 processors using the time domain method.

4. CONCLUSIONS

In this paper, the numerical investigations of the effect of the flutter instabilities of the blade on the unsteady flow inside T106A turbine are conducted using a high-fidelity DNS method. First of all, the CFD model used in this paper is validated against the experiment as well as the previous DNS simulations in terms of time-averaged pressure coefficient distribution, wake profile and wall shear stress. Using the validated CFD model, the effects of the flutter instability of the blade on the unsteady flow in this turbine are investigated based on two IBPAs, zero degree and 180 degrees, in terms of time-averaged pressure coefficient distribution, wake profile and vorticity field. Results obtained show that the unsteady flow field is highly distorted by the blade vibration and the rate of impact depends on the section of the blade, the amplitude of vibration and the IBPA. In the case of zero degree IBPA, a recurring

pattern of vortex formation is observed with the flow mixed up in the far downstream region. However, in the case of 180 degrees IBPA, the flow structures produced by the upper blade approach the lower blade soon after they shed from the trailing edge and mix up with those from the lower blade forming the turbulent wake and affecting the wake profiles in the downstream region. The flow unsteadiness and turbulence are higher at the blade outer sections in both cases, but the magnitudes are much greater in the 180 degrees IBPA case. Positive aerodynamic damping values are obtained for all IBPAs considered in this study, but it is larger at higher IBPAs. Therefore, it can be concluded that the aeroelastic instability of the blade has a direct and significant impact on the unsteady flow dominating the wake forming process in the downstream region.

In addition to the time domain method, the harmonic balance method using different harmonics is also used in this paper to determine the capability of the method in analysing aeroelasticity and unsteady flow in a modern LPT. Results show that at least 5 harmonics are required to resolve the necessary flow structures. The unsteady pressure amplitude coefficient and phase angle obtained from the time domain method and the harmonic balance method are in very good agreement. In terms of computation time, the 180 degrees IBPA case requires a larger amount of CPU time as two passages are required. Although the harmonic balance method solves considerably faster than the time domain method even when using a smaller number of processors, this method requires a significant amount of computational resources compared to the time domain method and the use of higher numbers of harmonics is limited for these particular cases using the DNS method.

ACKNOWLEDGEMENTS

The authors would like to acknowledge the financial support received from the Engineering Physics and Science Research Council of the UK (EPSRC EP/R010633/1).

REFERENCES

1. Hodson H, Howell R (2005) The role of transition in high-lift low-pressure turbines for aeroengines, Progress in Aerospace Sciences 41(6), 419–454.

2. Himmel C.G. (2010) Ultra-High lift blades for Low Pressure Turbines. PhD Thesis, University of Cambridge.

3. Hodson, H., Howell R., (2005) Blade Row Interactions, Transition, and High-Lift Aerofoils in Low-Pressure Turbines, Annu. Rev. Fluid Mech. 37, 71–98.

4. Cull J, Hodson H (2011) Unsteady boundary-layer transition in low-pressure turbines, J. Fluid Mech., 681(1), 370–410.

5. Panovsky J, Kielb, R.E (2000) A Design Method to Prevent Low Pressure Turbine Blade Flutter; J. Eng. Gas Turbines Power; 122(1): 89-98.

6. Waite J.J, Kielb R.E (2014) Physical Understanding and Sensitivities of Low Pressure Turbine Flutter; J. Eng. Gas Turbines Power; 137(1): 012502.

7. Waite J.J, Kielb R.E (2015) The Impact of Blade Loading and Unsteady Pressure Bifurcations on Low-Pressure Turbine Flutter Boundaries; ASME. J. Turbomach.; 138(4): 041002.

8. Corral, R. and Vega, A. (2016) The Low Reduced Frequency Limit of Vibrating Airfoils—Part I: Theoretical Analysis, ASME J. Turbomach., 138(2), 021004.

9. Dowell E. (2015) A Modern Course in Aeroelasticity, Springer, ISBN 978-3-319-09452-6.

10. Ning W, He L (1998) Computation of Unsteady Flows Around Oscillating Blades Using Linear and Nonlinear Harmonic Euler Methods, ASME J. Turbomach 120(3), 508-514.

11. Hall K, Lorence C (1993) Calculation of Three-Dimensional Unsteady Flows in Turbomachinery Using the Linearized Harmonic Euler Equations, ASME J. Turbomach., 115(4), pp. 800-809.

12. Hall K, Thomas J, Clark W (2002) Computation of Unsteady Nonlinear Flows in Cascades Using a Harmonic Balance Technique, AIAA Journal, 40(5), pp. 879-886.

13. He L (2008) Harmonic Solution of Unsteady Flow Around Blades with Separation, AIAA Journal, 46, (6), pp. 1299-1307.

14. Rahmati M.T, He L, Wells R.G (2010) Interface treatment for harmonic solution in multi-row aeromechanic analysis, ASME Turbo Expo 2010: Power for Land, Sea, and Air (pp. 1253-1261). American Society of Mechanical Engineers.

15. Rahmati M.T, He L, and Li Y.S (2012) Multi-row interference effects on blade aeromechanics in compressor and turbine stages, 13th International Symposium on Unsteady Aerodynamics, Aeroacoustics and Aeroelasticity of Turbomachines (ISUAAAT), September 11-14, Tokyo, Japan.

16. Rahmati M.T, He L, and Li Y.S (2016) The Blade Profile Orientations Effects on the Aeromechanics of Multirow Turbomachines, J. Eng. Gas Turbines Power, 137 (6), 062606.

17. Rahmati M.T, He L, Wang D.X, Li Y.S, Wells R.G, Krishnababu S.K (2014) Nonlinear Time and Frequency Domain Methods for Multirow Aeromechanical Analysis, ASME J. Turbomach., 136(4), 041010.

18. Win Naung S, Rahmati M.T, Farokhi H (2019) Aerodynamic Analysis of a Wind Turbine with Elevated Inflow Turbulence and Wake using Harmonic Method; Proceedings of the ASME 2019 38th International Conference on Ocean, Offshore and Arctic Engineering (OMAE2019); June 9-14, Glasgow, Scotland.

19. Win Naung S, Rahmati M.T, Farokhi H (2019) Aeromechanical Analysis of Wind Turbines using Non-linear Harmonic Method; Proceedings of the ASME 2019 38th International Conference on Ocean, Offshore and Arctic Engineering (OMAE2019); June 9-14, Glasgow, Scotland.

20. Tucker P.G (2001) Computation of unsteady internal flows. Norwell MA: Kluwer Academic Publishers.

21. Tucker P.G (2005) Computation of unsteady turbomachinery flows: Part 1—Progress and challenges, Progress in Aerospace Sciences, 47(7), 522-545.

22. Tucker P.G (2013). Unsteady computational fluid dynamics in aeronautics, Springer, ISBN 978-94-007-7048-5.

23. Stadtmüller P (2001) Investigation of wake-induced transition on the LP turbine cascade T106A-EIZ, DFG-Verbundproject Fo 136/11, Version 1.0.

24. Wang Y.F, Chen F, Liu H.P, Chen H.L (2014) Large eddy simulation of unsteady transitional flow on the low-pressure turbine blade, China Technol. Sci., 57(9): 1761–1768.

25. Garai A, Diosady L.T, Murman S.M, Madavan N.K (2016) DNS of Low-Pressure Turbine Cascade Flows With Elevated Inflow Turbulence Using a Discontinuous-Galerkin Spectral-Element Method, Proceedings of the ASME Turbo Expo 2016: Turbomachinery Technical Conference and Exposition, June 13–17, Seoul, South Korea.

26. Wissink J.G (2003) DNS of separating, low Reynolds number flow in a turbine cascade with incoming wakes, Int. J. of Heat and Fluid Flow, 24(4), 626-635.

27. Wissink J.G, Rodi, W (2006) Direct Numerical Simulations of Transitional Flow in Turbomachinery, ASME J. Turbomach., 128 (4), 668–678.

28. Michelassi V, Wissink J, Rodi W (2002) Analysis of DNS and LES of Flow in a Low Pressure Turbine Cascade with Incoming Wakes and Comparison with Experiments, Flow, Turbulence and Combustion, 69: 295–330.

29. Ranjan R, Deshpande S.M, Narasimha R (2017) New insights from high-resolution compressible DNS studies on an LPT blade boundary layer, Computers and Fluids, 153: 49–60.

30. Sandberg R.D, Michelassi V, Pichler R, Chen L, Johnstone R (2015) Compressible Direct Numerical Simulation of Low-Pressure Turbines—Part I: Methodology, ASME. J. Turbomach, 137(5): 051011.

31. Michelassi V, Chen L, Pichler R, Sandberg R.D (2015) Compressible Direct Numerical Simulation of Low-Pressure Turbines—Part II: Effect of Inflow Disturbances, ASME. J. Turbomach, 137(7): 071005.